







Please cite the Published Version

McGrath, Alexander J , Wadge, Matthew D , Adams, Marcus , Manickam, Kandavel, Ling, Sanliang , Walker, Gavin S  and Grant, David M  (2024) Stoichiometry and annealing condition on hydrogen capacity of TiCr_{2-x} AB₂ alloys. International Journal of Hydrogen Energy, 53. pp. 582-591. ISSN 0360-3199

DOI: <https://doi.org/10.1016/j.ijhydene.2023.12.062>

Publisher: Elsevier

Version: Published Version

Downloaded from: <https://e-space.mmu.ac.uk/635553/>

Usage rights:  [Creative Commons: Attribution 4.0](https://creativecommons.org/licenses/by/4.0/)

Additional Information: This is an open access article which first appeared in International Journal of Hydrogen Energy

Enquiries:

If you have questions about this document, contact openresearch@mmu.ac.uk. Please include the URL of the record in e-space. If you believe that your, or a third party's rights have been compromised through this document please see our Take Down policy (available from <https://www.mmu.ac.uk/library/using-the-library/policies-and-guidelines>)



Stoichiometry and annealing condition on hydrogen capacity of $\text{TiCr}_{2-x}\text{AB}_2$ alloys

Alexander J. McGrath^{*}, Matthew D. Wadge, Marcus Adams, Kandavel Manickam, Sanliang Ling, Gavin S. Walker, David M. Grant^{**}

Advanced Materials Research Group, Faculty of Engineering, University of Nottingham, UK

ARTICLE INFO

Handling Editor: Dr Z Sun

Keywords:
Hydrogen storage
Metal hydrides
 AB_2 alloys
TiCr

ABSTRACT

This study presents the effect of stoichiometry and annealing condition on Ti–Cr AB_2 -type hydrogen storage alloys. Prior to annealing the majority phase of the as-cast alloys was the C14 Laves phase, with separate Ti and Cr phases. Annealing treatment (1273 K/14 d) led to a transition from C14 to C15 Laves phase structure. Both C14 (as-cast) and C15 (annealed) cell size increased with Ti content, up to a ratio (Cr/Ti) of 1.6, due to B-site Ti substitution in the lattice up to a limit. Pressure composition isotherm (PCI) measurements demonstrated alloys containing a greater Ti content had a better maximum hydrogen storage capacity (1.5 vs. 1.03 wt%) and lower plateau pressure (9.4 vs. 15.8 bar) at 253 K. Annealing resulted in a lower storage capacity (1.05 vs. 1.49 wt%), greater plateau pressure (ca. 30 bar) and flatter plateau slope (25 % reduction in plateau slope). Reduction in hydrogen storage capacity of annealed alloys could be due to diffusion of residual Cr in the alloy into the C15 Laves phase during the annealing process, thereby changing the local composition as confirmed through X-ray diffraction (XRD).

1. Introduction

Storing hydrogen in a safe and efficient manner is arguably one of the most significant barriers to implement hydrogen as a low-carbon energy vector across the globe. Solid-state storage of hydrogen offers a less energy intensive, safer, and volumetrically more efficient method of storing hydrogen. Intermetallic compounds form a significant proportion of materials that have been explored for solid-state hydrogen storage. Some of the families of compounds that have been well researched over the last few decades include the AB, AB_2 and AB_5 alloys, due to their versatility in terms of composition and properties [1–10]. The typical components in each of the alloy families can vary, with transition metals such as Ti, Mn, Cr, being more common in the AB and AB_2 family, and rare earths such as La, Ce, Nd being more common in the AB_5 family, particularly in the A site [11]. A focus in recent years has been put towards researching the AB_2 family of alloys due to their versatility in composition and ambient temperature PCI capabilities [12].

Ti and Cr have been used frequently in AB_2 alloys, as the hydrogen storage properties of the AB_2 compound TiCr_2 are well known, where research into this particular compound dates back as early as the 1970s

where it was found that up to 0.8 wt% of hydrogen could be absorbed at 20 °C by Machida et al. [13]. Johnson and Reilly also conducted several studies into the hydrides of TiCr_2 and $\text{TiCr}_{1.8}$, where temperatures as low as 213 K were needed to observe a flat plateau. At these temperatures, the Ti–Cr alloys were seen to have multiple plateaux [14–16]. Due to the very high plateau pressures of Ti–Cr AB_2 alloys at ambient conditions, this system is suited more towards use in metal hydride hydrogen compressors. Research in the past decade has involved modifying the TiCr_2 composition for metal hydride compression applications, by alloying with other transition metals including Zr, Mn, Fe and V. The range of theoretical substitutions into the A and B site of TiCr_2 that can be done to affect the formation energies and enthalpy of hydrogenation is extensive as shown by Loh et al. [17]. Li et al. have shown that a suitable alloy for an intermediate stage in a metal hydride compressor can be made by alloying with Zr and Fe, with a reversible capacity of 1.4 wt% at –20 °C and minimal hysteresis [18]. Cao et al. have further demonstrated that the Ti–Zr–Cr–Fe AB_2 alloy system can have metal hydride compressor applications at more moderate working temperatures by alloying with V, improving the hydrogen storage capacity to 1.52 wt% at 20 °C whilst still maintaining a flat plateau and very little

^{*} Corresponding author.

^{**} Corresponding author.

E-mail addresses: alexander.mcgrath@nottingham.ac.uk (A.J. McGrath), david.grant@nottingham.ac.uk (D.M. Grant).

<https://doi.org/10.1016/j.ijhydene.2023.12.062>

Received 26 September 2023; Received in revised form 22 November 2023; Accepted 7 December 2023

Available online 18 December 2023

0360-3199/© 2023 The Authors. Published by Elsevier Ltd on behalf of Hydrogen Energy Publications LLC. This is an open access article under the CC BY license (<http://creativecommons.org/licenses/by/4.0/>).

hysteresis [19]. Another alternative to this solution for moderate compression is to alloy with Mn and Fe as demonstrated by Chen et al., achieving a hydrogen storage capacity of 1.78 wt% at -30°C with very little plateau slope [1]. Whilst these examples are aimed at intermediate compression pressures (20–45 MPa), the Ti–Zr–Cr–Fe–V system has also been shown by Wang et al. to be useful in the second stage for higher pressure compression (up to 70 MPa) by fine-tuning the composition [20].

There are three main phases that can be found within the TiCr_2 alloy, the hexagonal C14 and C36 Laves phases, and the cubic C15 Laves phase. The C14 and C15 Laves phases are more commonly formed compared to the C36 phase, however each of the three phases can be attained according to the Ti–Cr phase diagram (Fig. 1). Annealing of an alloy is an effective method of homogenising a specific crystal structure. This has been demonstrated for hydrogen storage purposes with Zr-based AB_2 alloys where annealing at temperatures increasing up to 1100°C correlated to a higher phase percentage of the C14 and C15 Laves phases within the alloys, depending on the composition [21]. The C15 Laves phase has a greater theoretical maximum storage capacity of 7 H atoms per AB_2 unit, compared to the 6.33 H atoms per AB_2 unit of the C14 Laves phase according to Young et al. [22]. However, Shoemaker et al. states the converse with the theoretical maximum being 6 and 6.33, respectively [23]. Despite this, it has been demonstrated for multicomponent AB_2 alloys that the critical hydrogen storage parameters such as gravimetric capacity and plateau pressure are dependent on the chemical and structural composition of the alloy. In particular, whether the C14 or C15 phase is dominant in the alloy [22,24].

Whilst a significant amount of research has focused around stoichiometric AB_2 , more recent experiments have shown the enhancement of hydrogen storage properties in AB_2 alloys through off-stoichiometric compositions. Alloys that are rich in either the A or B component can cause site vacancies within the lattice, which are either filled by the excess A/B atoms or are left vacant. This results in the lattice expanding or contracting. This has been successful with Ti-based AB_2 alloys, where a stoichiometric increase from 1 up to 1.1 has resulted in lattice expansion due to the larger atomic radius of Ti, and therefore an increased hydrogen storage capacity [3,25]. Off-stoichiometry can also be used to tune other storage properties, such as hydrogenation enthalpy

and plateau pressure, which is critical for end-use applications such as hydrogen fuel cell and metal hydride compressors.

Off-stoichiometry in Ti–Cr AB_2 alloys has been researched previously outside the area of hydrogen storage, where the observed microstructures were linked to the mechanical properties of the alloys by Chen et al. [27]. As the compositions move away from the TiCr_2 stoichiometry, changes in cell volume are attributed to either substitution of Cr by Ti in B-sites, or Cr vacancies within the lattice. Analysis of the lattice parameters as per the data presented in Fig. 2 for the C36 Laves phase shows a greater cell volume as Ti content increases, which led to the conclusion that Ti substitution is a more likely result in off-stoichiometric alloys. There is however a noticeable plateau in the cell parameters when the alloy composition is < 64 and > 67 at% Cr, which suggests that there could be a limit to which Ti can substitute for Cr in the Laves phase structures. The substitution of Ti into the B-site of the C36 TiCr_2 Laves phase has also been verified more recently by Baumann and Leineweber, concluding that Ti substitution is the dominant mechanisms and that Cr vacancies are much less common in the Ti-rich C36 phase [28].

The method used to synthesise Ti–Cr alloys has a significant influence on the observed phases. Biffi et al. have previously synthesised $\text{TiCr}_{1.78}$ which contained Laves and metallic phases from Ti and Cr powders using selective laser melting, whereas Murashkina et al. produced a singular C36 phase from powders using abnormal glow discharge plasma [29,30]. It is also known that arc melting can produce metal alloy samples with a mixture of different phases due to fast cooling. To fully understand the effect of the additional phases and unreacted metals on the hydrogen storage properties, it is therefore desired to produce a single intermetallic phase in the Ti–Cr alloys through annealing. The C15 phase was selected as the target phase due to the wide composition range available at the appropriate temperature, according to the Ti–Cr phase diagram. A detailed comparison can then be made between the as-cast sample (with a mixture of different phases) and the annealed sample (featuring single C15 phase) on the hydrogen storage capacity and plateau pressure of the Ti–Cr alloys.

The studies detailed in this paper were undertaken in order to understand the changes in structural characteristics and hydrogen storage properties of several off-stoichiometric variations of the TiCr_2 binary composition. The atomic ratio of Cr at the B site of the alloys made ranged between 1.55 and 1.85. As far as off-stoichiometric Ti–Cr binary compositions for hydrogen storage are concerned, there is very little prior research involving compositions rich in Ti at the time of completing this study. Previous work involving binary Ti–Cr AB_2 alloys for hydrogen storage has been mostly done using temperatures below 0°C due to the high plateau pressures at ambient temperatures [14].

2. Materials and methods

2.1. Alloy preparation

The raw materials used to form each of the alloys were Ti sponge and Cr pieces, purchased from Alfa Aesar (both $> 99.2\%$ purity). The alloys weighing ca. 10 g were melted into buttons by arc melting (Edmund Bühler GmbH compact Arc Melter MAM-1) under an inert (Ar) atmosphere, using a water-cooled copper crucible. Each alloy was flipped and re-melted thrice to achieve a homogeneous composition throughout the button. The buttons were then mechanically crushed into small pieces, no more than 2–3 mm in diameter. Some pieces were crushed further into a powder for hydrogenation measurements, Scanning Electron Microscopy (SEM) and X-ray diffraction (XRD), whilst the rest was set aside for annealing.

2.2. Annealing conditions

Two separate annealing processes were used to achieve a single phase within the alloy samples, with one anneal taking place for 2.5 days

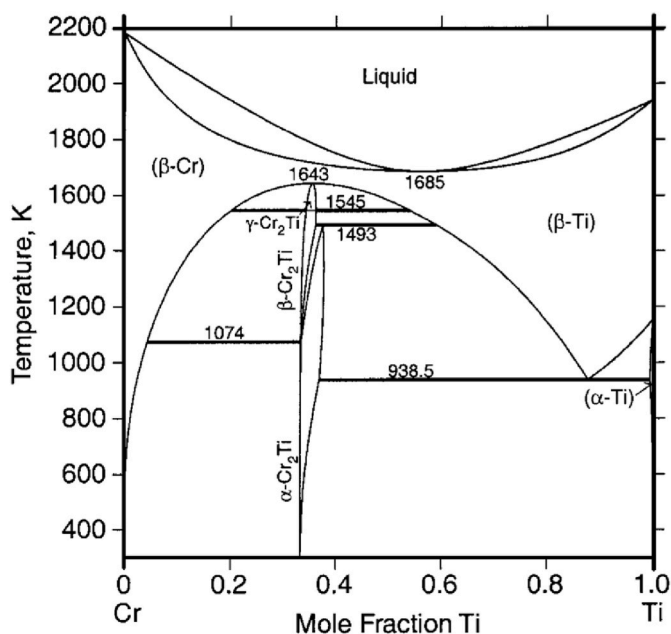


Fig. 1. Ti–Cr phase diagram. $\alpha\text{-TiCr}_2$ corresponds to the C15 Laves phase, $\beta\text{-TiCr}_2$ corresponds to C14, and $\gamma\text{-TiCr}_2$ corresponds to C36. Reproduced with permission from Springer [26].

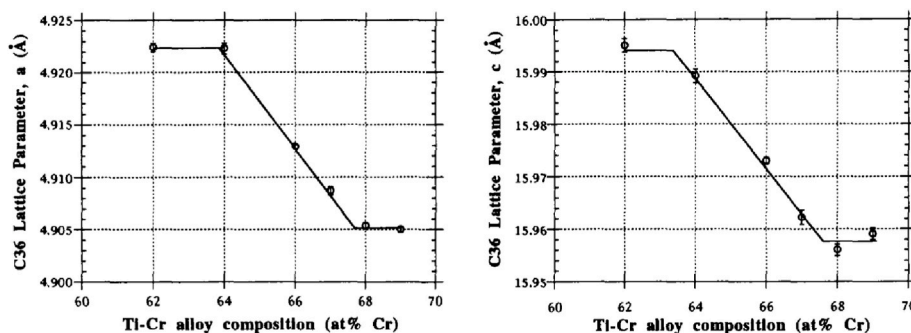


Fig. 2. C36 lattice parameters of Ti-Cr AB2-based alloys. Reproduced with permission from Springer Nature [27].

at 1073 K, and the other for a 2-week period at 1273 K. All samples were contained in a quartz ampoule sealed with Ar gas. The selection of the annealing temperatures was based on the Ti-Cr phase diagram, with the aim of producing a single C15 phase in the Ti-Cr alloy samples. It is noted that annealing was carried out for a long period of time (2 weeks) due to the extremely slow kinetics of the C14/C36 to C15 transition, which is also described by Baumann et al., and Johnson and Reilly [14, 28]. The annealing temperatures were selected so that the alloy compositions would sit in the C15 region of the Ti-Cr phase diagram.

2.3. Materials characterisation

Pieces were mounted and polished, to be examined using scanning electron microscopy (SEM). These pieces were also etched using Kroll's reagent (92 % H₂O, 6 % HNO₃, 2 % HF by volume) to reveal the grain boundaries within the alloy. Microstructural characterisation and composition analysis was carried out using a JEOL 6490LV SEM, equipped with an Oxford instruments energy dispersive x-ray detector (EDX) for elemental analysis. Images of the alloys were taken in secondary electron (SE) mode to examine the surface topography, and also in backscatter electron (BSE) mode to explore the phase distribution amongst each of the alloys.

The structural parameters of the alloys were determined from the powder X-ray diffraction patterns taken using a D8 Bruker aXS Advance X-ray diffractometer with Cu K α radiation, and $\lambda = 1.5406$ Å. Each scan was completed over a 2θ range of 20–135°, with a step size of 0.02° and a time of 0.6 s per step. Critical structural parameters of the as-cast and annealed alloys, including phase quantification, lattice parameters and occupancy factors were calculated *via* Rietveld refinement on each of the measured diffraction patterns using TOPAS-Academic software.

The parameters that were allowed to refine were carefully selected so that an accurate structural description of each alloy could be produced. Firstly, a correction was allowed to be made for the instrument background, zero point and height of the sample being analysed. For the major Laves phase in each alloy (C14, C15), lattice parameters and Cr occupancy at the B site were allowed to refine. Ti occupancy at the A site was fixed at 1 due to the Ti-rich nature of the alloys. A Ti parameter for the B site was also introduced to determine the amount of B-site substitution that was taking place, this value was allowed to refine from a first estimate of 0.05. Temperature factors for all phases remained constant across all phases, using the values calculated from the refinements of the TiCr_{1.55} alloy samples. Each phase was allowed to have a peak shape refined. Lattice parameters and occupancy factors for the Ti and Cr single phases remained constant.

2.4. Hydrogen uptake

Hydrogen absorption/desorption and pressure-composition isotherm (PCI) measurements were taken using a calibrated Sievert's volumetric apparatus [31]. The manifold and sample holder volumes of the Sievert's apparatus were 48.096 cm³ and 13.045 cm³, respectively.

The preparation procedure was kept the same for each of the alloys produced during the study. Approximately 1 g of each alloy was crushed into fine particles, the samples were then weighed and loaded into the sample vessel in an inert atmosphere. The sample vessel was then removed of all gases and one full hydrogenation cycle at *ca.* 300 K using *ca.* 100 bar of hydrogen (manifold pressure) was carried out to fully activate the material, with an activation time of at least 60 min. A further minimum of three additional cycles were then completed to ensure that a consistent weight percentage of hydrogen was being taken up and released. All samples activated easily. Activation took place under *ca.* 75 bar hydrogen and at 300 K. The PCI measurements were performed between the pressures of 0–100 bar and at temperatures of 253 K and 300 K. Temperatures of 253 K for PCI measurements were reached using a salt and ice bath, which was regularly agitated and in which the sample holder was fully submerged so that a consistent temperature throughout the entire sample holder was maintained. The manifold temperature was maintained constant at 298 K during low temperature experiments using a PID controlled heater in an enclosed environment. A separate volume calibration at 253 K was carried out after each PCI measurement in order to quantify the hydrogen uptake as accurately as possible. Prior to each PCI experiment the sample was evacuated using a turbo molecular pump backed by a diaphragm pump.

3. Results

3.1. As-cast alloys

XRD patterns of the as-cast alloys (shown in Fig. 3) reveal a multi-phase structure present within each of the alloys. Peak indexing reveals that the most abundant phase is the C14 Laves phase, however minor HCP-Ti and BCC-Cr phases, located at $2\theta = 40^\circ$ and 44° , respectively, can also be seen. The C14 and C36 Laves phases share the majority of their peaks due to their structural similarities, with the C36 phase having very few unique peaks. These have been identified at *ca.* $2\theta = 21.5^\circ$, 47.7° , and 80° . Whilst there is likely a small percentage of C36 phase present, it is very difficult to quantify this through Rietveld refinement. Similar difficulties have also been found with phase quantification of C14/C36 by Biffi et al. and Coduri et al. [29,32]. For the duration of the study, it is assumed that the dominant Laves phase in the as-cast alloys is the C14 phase, which is shown in results from Rietveld refinement. The quantities of each phase in the as-cast Ti-Cr alloys, calculated from a Rietveld refinement of the XRD patterns, are available in Table 1.

The unit cell volume for the C14 phase in each of the as-cast alloys has been calculated from Rietveld refinement, the results from this analysis, as well as referenced TiCr₂ stoichiometric cell volumes taken from the Crystallography Open Database (COD) and the International Centre for Diffraction Data (ICDD), are displayed in Fig. 4. The unit cell volume increases from 167.3 Å³ to 168.0 Å³ as the Cr ratio decreases from 1.85 to 1.55. There is notably an initial decrease between both referenced TiCr₂ cell volumes (168.6 Å³ from COD (1525361) and 167.7

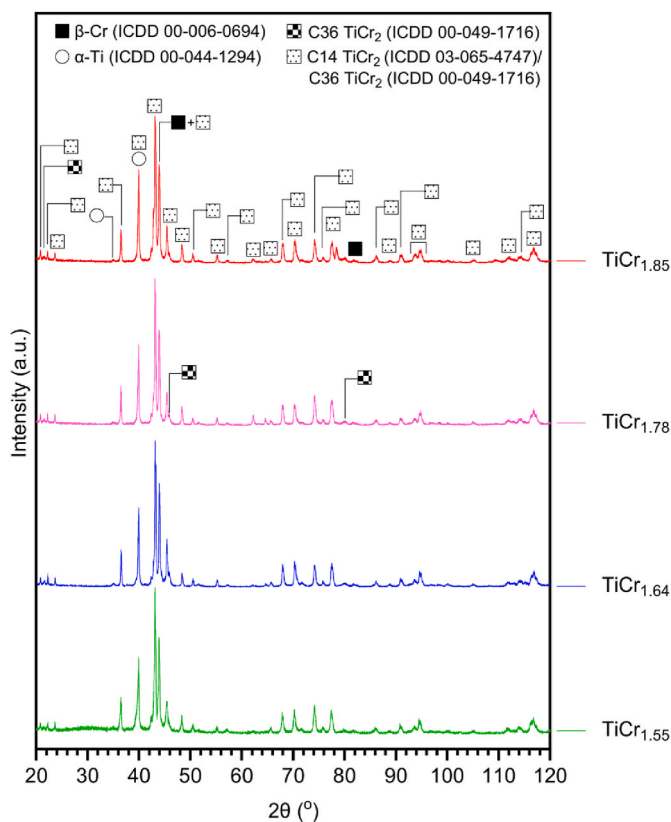


Fig. 3. XRD patterns of as-cast $\text{TiCr}_{1.55}$ - $\text{Ti}_{1.85}$ alloys.

Table 1

Atomic site occupancies of the C14 phase in the as-cast Ti–Cr alloys as calculated via Rietveld refinements. B1 and B2 refers to the B-sites available in the C14 lattice, which are occupied by both Ti and Cr in off-stoichiometric alloys.

Alloy	C14 site occupancies			
	Cr(B1)	Cr(B2)	Ti(B1)	Ti(B2)
$\text{TiCr}_{1.55}$	0.797	0.810	0.0197	0.0134
$\text{TiCr}_{1.64}$	0.832	0.838	0.0283	0.00966
$\text{TiCr}_{1.78}$	0.836	0.831	0.0150	0.00503
$\text{TiCr}_{1.85}$	0.838	0.851	0.0134	0.00594

Å^3 from ICDD (03-065-4747)) and the calculated $\text{TiCr}_{1.85}$ cell volume (167.3 Å^3).

Additional results from Rietveld refinements of the as-cast alloys are provided, including the occupancy factors of Ti and Cr in the B-sites of the C14 lattice in Table 1, and the phase percentages present in each alloy are given in Table 2. Data from Table 1 shows a decrease in Cr occupancy in both B-sites as the alloy becomes richer in Ti from $\text{TiCr}_{1.85}$ to $\text{TiCr}_{1.55}$, where B1 Cr site occupancy decreases from 0.838 to 0.797 and B2 Cr site occupancy decreases from 0.851 to 0.810. Whilst the Cr occupancy decreases, the Ti occupancy increases from 0.0134 to 0.0197 in the B1 site and from 0.00594 to 0.0134 in the B2 site. The trend does however deviate in the case of the $\text{TiCr}_{1.64}$ alloy, where the Ti occupancy overall is at its greatest, as well as an increase in Cr occupancy in comparison to the $\text{TiCr}_{1.78}$ alloy. Table 2 shows that the phase percentage of the C14 Laves phase increases as the alloy becomes richer in Cr, from 84.5 % in the $\text{TiCr}_{1.55}$ alloy to 89.2 % in the $\text{TiCr}_{1.85}$ alloy, while the phase percentage of Ti simultaneously decreases from 5.5 % to 3.1 %.

SEM micrographs and EDX maps of the as-cast alloys are shown in Fig. 5. Images of the etched samples in SE mode reveal a dendritic structure, which is particularly prominent in the $\text{TiCr}_{1.55}$ and $\text{TiCr}_{1.64}$

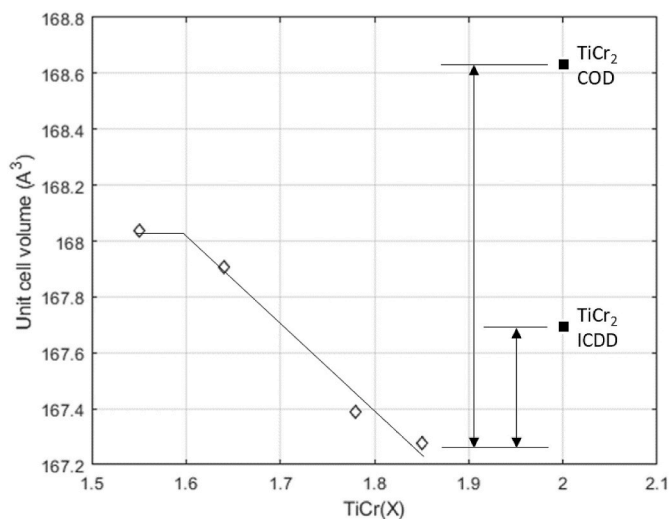


Fig. 4. Unit cell volume of C14 Laves phase in as-cast alloys calculated from Rietveld refinement with reference TiCr_2 C14 cell volume. COD (1525361) and ICDD (03-065-4747) database values added for stoichiometric TiCr_2 values.

Table 2

Phase percentages of as-cast Ti–Cr alloy as determined via Rietveld refinement of the XRD spectra. The quantity of the phases corresponds to the best fit, which employs the least squares method to reduce the total residual.

Alloy	C14 wt%	Ti wt%	Cr wt%
$\text{TiCr}_{1.55}$	84.51	5.48	10.01
$\text{TiCr}_{1.64}$	85.04	4.54	10.42
$\text{TiCr}_{1.78}$	86.32	4.20	9.48
$\text{TiCr}_{1.85}$	89.15	3.12	7.73

alloys (Fig. 6). The incidence of Ti-rich areas can be seen to decrease as the composition of the alloy decreases in Ti. Spot analysis in Ti-rich and bulk areas was also carried out to quantify the Ti/Cr ratio in each area, as well as to discover if any oxygen was present as a contaminant. The results from the spot analysis are discussed in more detail in the annealed section and are summarised in Table 6.

The pressure-composition isotherms (PCIs) for hydrogenation were carried out at 300 K and 253 K as shown in Fig. 7. The full extent of the $\alpha+\beta$ and the β phase for PCI measurements could not be achieved with the pressure limit on the apparatus of 100 bar at 300 K. Therefore, a lower temperature was required to measure a full hydrogenation plateau. The temperature was therefore reduced to 253 K, and the PCI measurements at this temperature for the as-cast alloys are shown in Fig. 7.

A summary of the hydrogen storage properties of the as-cast alloys are presented in Table 3. Results from hydrogenation measurements show a greater plateau and reduced hydrogen storage capacity as the Cr content in the alloy increases. The drop-off in capacity is much more severe as the stoichiometry moves closer towards TiCr_2 , with the maximum capacity at 100 bar H_2 reducing from 1.5 wt% to 1.36 wt% between $\text{TiCr}_{1.55}$ and $\text{TiCr}_{1.78}$, however the reduction between $\text{TiCr}_{1.78}$ and $\text{TiCr}_{1.85}$ is much greater with the maximum capacity for $\text{TiCr}_{1.85}$ at 100 bar is only 1.03 wt%. Therefore, for the remainder of this study, the $\text{TiCr}_{1.64}$ alloy was chosen as the focus composition due to since from the phase diagram, this composition sits close to the C15/C15+Ti boundary (Fig. 8), which from similar results with Ti–Mn alloys, will increase hydrogen storage performance due to it being on the Ti-rich side of the Laves phase according to Liu et al. [33].

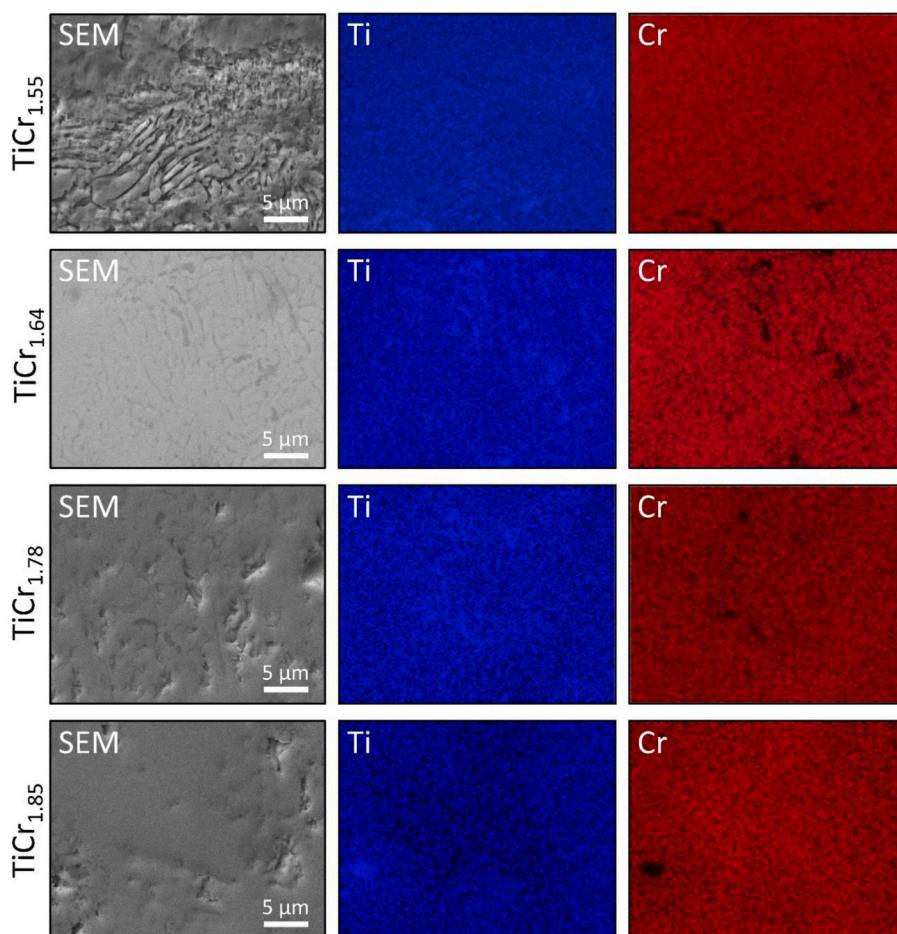


Fig. 5. SEM micrographs and EDX maps of all as-cast samples: $\text{TiCr}_{1.55}$, $\text{TiCr}_{1.64}$, $\text{TiCr}_{1.78}$, $\text{TiCr}_{1.85}$.

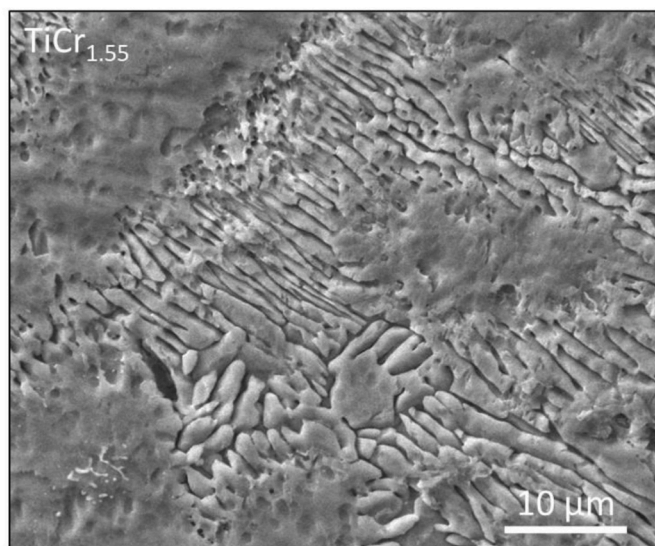


Fig. 6. Representative micrograph of the dendritic structure within the $\text{TiCr}_{1.55}$ alloy.

3.2. Annealed alloys

Samples of each alloy were annealed in order to achieve phase purity within the alloy microstructure and to reduce the plateau slope. The XRD patterns of samples annealed for 2.5 days at 1073 K and 14 days at

1273 K are compared against the as-cast sample for the $\text{TiCr}_{1.64}$ alloy in Fig. 9. The annealed samples show much sharper XRD peaks, with a reduction of FWHM from 0.235 to 0.115 consistent with the expected grain size increase and disordered boundary reduction, with the only Laves phase observed as the cubic C15. The peaks representative of the single metallic phases (Ti, Cr) at $\text{ca. } 2\theta = 40^\circ$ and $2\theta = 44^\circ$, respectively, can be seen to decrease in intensity between the as-cast and annealed samples, with the most reduction seen with the greater annealing times and temperatures.

Results from Rietveld refinement of the C15 phase in each of the alloys annealed at 1273 K for 14 days are given in Fig. 10. A similar trend is seen as that in Fig. 4, where the cell size increases with Ti content in the alloy (from 332.71 \AA^3 to 334.81 \AA^3). Once again, there is an initial decrease between calculated value for the $\text{TiCr}_{1.85}$ alloy and that of the stoichiometric TiCr_2 C15 cell size from the COD (336.3 \AA^3) and the ICDD (334.7 \AA^3). The calculated B-site occupancies of Ti and Cr are given in Table 4 for each of the Ti–Cr alloys annealed at 1273 K for 14 days. The $\text{TiCr}_{1.64}$ alloy has the most occupied Cr B-site with an occupancy of 0.934, with the remaining sites occupied by Ti or vacant. Note there is only one type of symmetry-unique Cr atom in C15. There is generally a greater Cr occupancy in the alloys richer in Ti, but there is no specific order followed for this parameter. The Ti B-site occupancy increases with Ti content in the annealed alloys, from 0.00347 in the $\text{TiCr}_{1.85}$ alloy to 0.0280 in the $\text{TiCr}_{1.55}$ alloy. Phase percentage data is also shown in Table 5, where the greatest percentage of the C15 phase is present in the $\text{TiCr}_{1.64}$ alloy (88.5 %). There is a small decrease of just under 4 % of the C15 phase from the $\text{TiCr}_{1.64}$ alloy to the $\text{TiCr}_{1.55}$ alloy, however in comparison there is a much more significant decrease in the C15% moving towards the $\text{TiCr}_{1.85}$ alloy (a decrease of ca. 17 %).

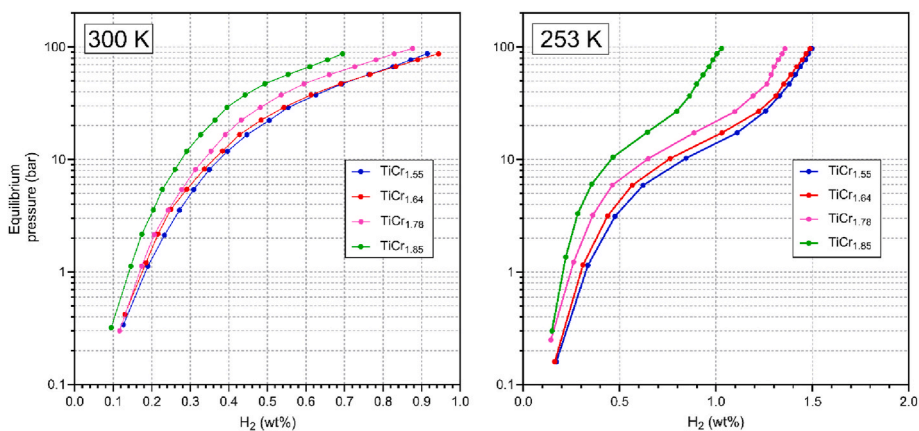


Fig. 7. Pressure-composition isotherms of as-cast alloys at 300 and 253 K, where hydrogen gas pressure is limited to 100 bar due to equipment.

Table 3
Summary of hydrogen storage properties of as-cast alloys at 253 K.

Alloy	H ₂ wt% @ 100 bar	P _{plateau} (bar)	H ₂ wt% @ P _{plateau}
TiCr _{1.55}	1.50 (±0.006)	9.4	0.8
TiCr _{1.64}	1.49 (±0.006)	11.2	0.8
TiCr _{1.78}	1.36 (±0.006)	14.7	0.8
TiCr _{1.85}	1.03 (±0.004)	15.8	0.6

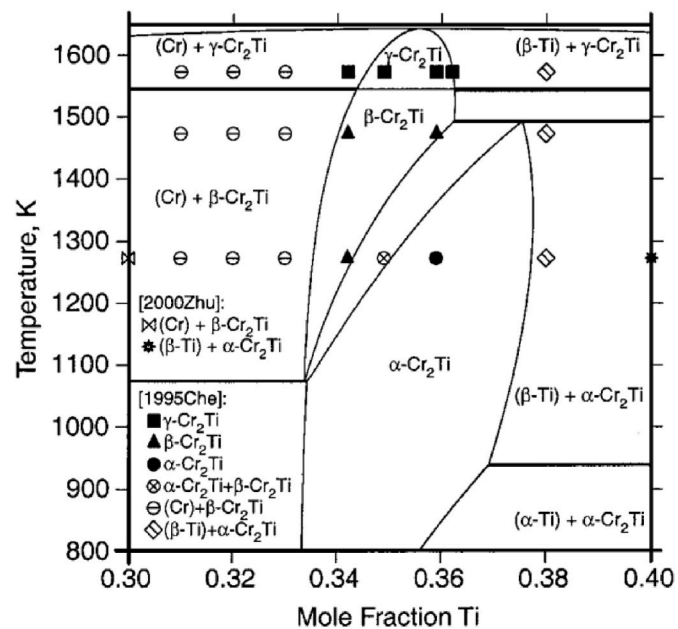


Fig. 8. Zoomed in region of the Ti–Cr phase diagram between 0.3 and 0.4 Ti mole fraction and 800–1600 K. Reproduced with permission from Springer [26].

SEM micrographs of the annealed TiCr_{1.64} alloy with the accompanying EDX maps are given in Fig. 11 with a comparison to those of the TiCr_{1.64} as-cast alloy. The Ti map highlights larger Ti-rich areas compared to those seen in the as-cast alloy. Spot analysis of Ti–Cr bulk and Ti-rich regions (illustrated by the arrows in Fig. 11) observed in both the as-cast and annealed TiCr_{1.64} alloys is given in Table 6. There is a sizeable O content in the Ti-rich regions in both alloys, with a significant increase from ca. 16.6 wt% in the as-cast to 23.3 wt% in the annealed alloy. The Ti content increases from 58.9 wt% in the as-cast to 72.2 wt% in the annealed alloy, verifying the observations from the EDX maps shown in Fig. 11. There is also a slight increase in Cr content in the Ti–Cr

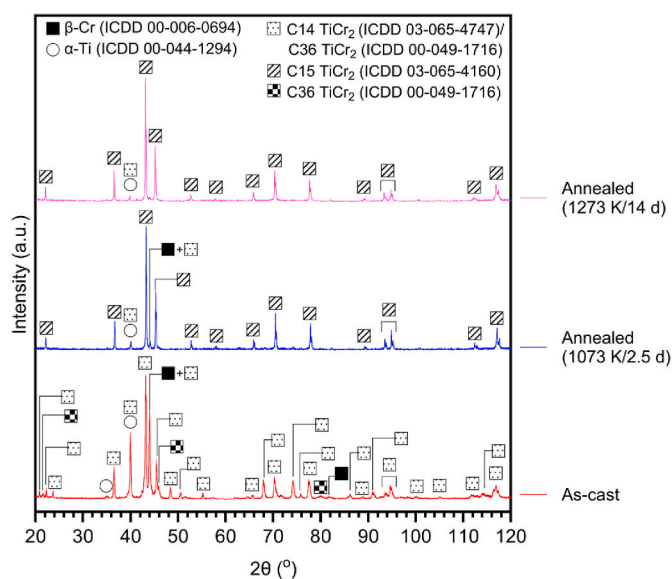


Fig. 9. XRD patterns of as-cast and annealed samples of the TiCr_{1.64} alloy.

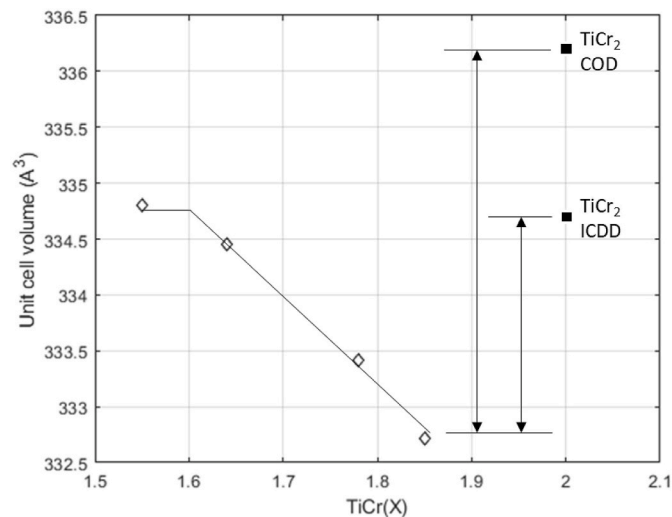


Fig. 10. Unit cell volume of C15 Laves phase in annealed alloys calculated from Rietveld refinement with reference TiCr₂ C15 cell volume. COD (1525360) and ICDD (PDF 03-065-4160) database values added for the stoichiometric TiCr₂ values.

Table 4

Atomic site occupancies of the C15 phase in the annealed Ti–Cr alloys.

Alloy	C15 site occupancies	
	Cr(B1)	Ti(B1)
TiCr _{1.55}	0.898	0.0280
TiCr _{1.64}	0.934	0.0138
TiCr _{1.78}	0.853	0.00621
TiCr _{1.85}	0.870	0.00347

Table 5

Phase percentages of annealed Ti–Cr alloys.

Alloy	C15 wt%	Ti wt%	Cr wt%
TiCr _{1.55}	84.57	6.10	9.33
TiCr _{1.64}	88.49	4.38	7.13
TiCr _{1.78}	79.04	7.76	13.20
TiCr _{1.85}	71.85	9.62	18.53

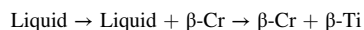
bulk regions, however it is noted that the slight increase in Cr weight percentage (from 63.96 wt% in the as-cast alloy to 64.49 wt% in the annealed alloy is within the error of the Cr weight percent in the as-cast alloy.

The hydrogen storage properties of the sample annealed at 1273 K for 14 days are compared to those of the as-cast sample in Fig. 12. Whilst the plateau has flattened somewhat, there is a clear reduction in storage capacity, from 1.05 to 1.49 wt% at ca. 97 bar, and a greater plateau pressure (ca. 30 bar difference) for the annealed sample.

4. Discussion

All the alloys studied are Ti-rich in stoichiometry. Upon examining the Ti–Cr phase diagram presented in Fig. 1, for the composition range of the alloys investigated (Ti mole fraction range 0.35–0.39) the first solids to form before reaching the Laves phase are β -Cr and β -Ti and not all of this is converted to the Laves phase, as observed in Table 2. The remaining β -Ti converts to the stable α -Ti; there is a small percentage of

β -Cr and α -Ti in the analysed results. It was determined that a specific path of phases was followed by each alloy during the transition from liquid to solid, before forming any of the Laves phases. This pathway predicted from the phase diagram (Fig. 1) is outlined below:



This pathway explains the presence of the small but significant α -Ti and β -Cr phases amongst the C14/C36 Laves phases that have been detected in the as-cast alloys from XRD. Annealing is therefore required when using this synthesis technique to obtain a phase-pure sample.

Rietveld refinement of the C14 phase in each alloy demonstrated an increase in cell volume as the Ti content in the alloy increased Fig. 4. Ti has a larger atomic radius than Cr, meaning that the increase in cell volume is due to the B-site substitution of Ti into the Cr site in the C14 lattice. It is however apparent that there is an initial drop-off in cell size in comparison to the stoichiometric TiCr₂ (Fig. 4). This could indicate that at smaller deviations away from stoichiometry (TiCr₂ to TiCr_{1.85} for example) that it is more energetically favourable to form Cr vacancies in the C14 lattice, before Ti substitution takes place as the composition becomes even more Ti-rich. Additionally, there may also be an upper limit to the amount of Ti substituting into the lattice, as there is very little increase in cell volume between TiCr_{1.64} and TiCr_{1.55}. The trend observed in Fig. 4 is very similar to that seen to the mechanical study by Chen et al. [27]. However, depending on the diffraction data source used, the observed drop from stoichiometric to sub-stoichiometric is significantly different. In this study the authors detailed the variance between diffraction data from the ICDD and COD databases for the same C14 phase structure, as well as the C15 phase for the annealed samples. It must be noted that some variance is expected from phase quantification depending on whether the material is single crystal, if there is any variance in crystal formation, the quality of the presented data, and the parameters in which the sample has been analysed. In this instance, the authors have used the highest quality phases possible to provide a better comparison. The COD database entry (1525360) presents a significant drop from the stoichiometric cell volume (168.8 Å³) compared to the ICDD (167.7 Å³) entry (03-065-4747), approximately a 1 Å³ difference, in relation to the TiCr_{1.85} sample. The ICDD database reference was from

Table 6Average compositions of Ti–Cr bulk and Ti-rich areas in the TiCr_{1.64} as-cast and annealed alloys.

Alloy	Ti–Cr bulk			Ti-rich		
	Ti (wt%)	Cr (wt%)	O (wt%)	Ti (wt%)	Cr (wt%)	O (wt%)
TiCr _{1.64} as-cast	36.04 (±0.81)	63.96 (±0.81)	0.00	58.86 (±2.25)	24.56 (±3.41)	16.58 (±1.29)
TiCr _{1.64} annealed	35.51 (±0.04)	64.49 (±0.04)	0.00	72.22 (±1.52)	4.52 (±0.94)	23.26 (±1.16)

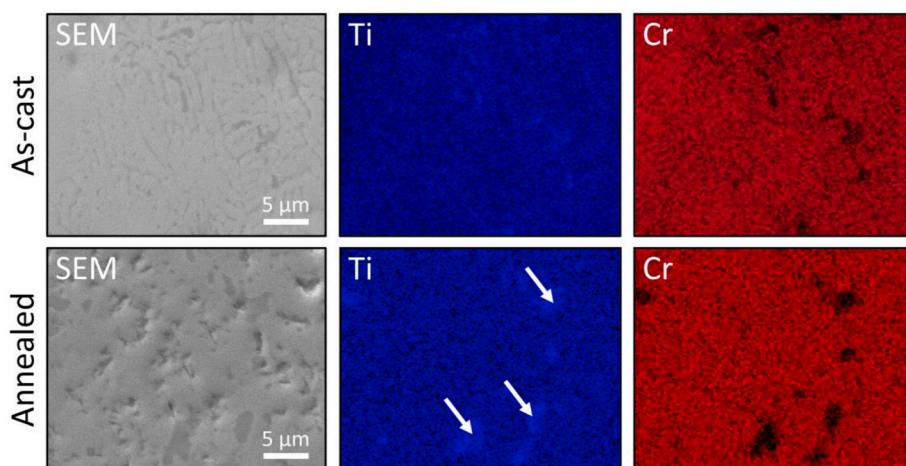


Fig. 11. SEM and EDX micrographs of as-cast and annealed (1273 K for 14 d) of a TiCr_{1.64} sample.

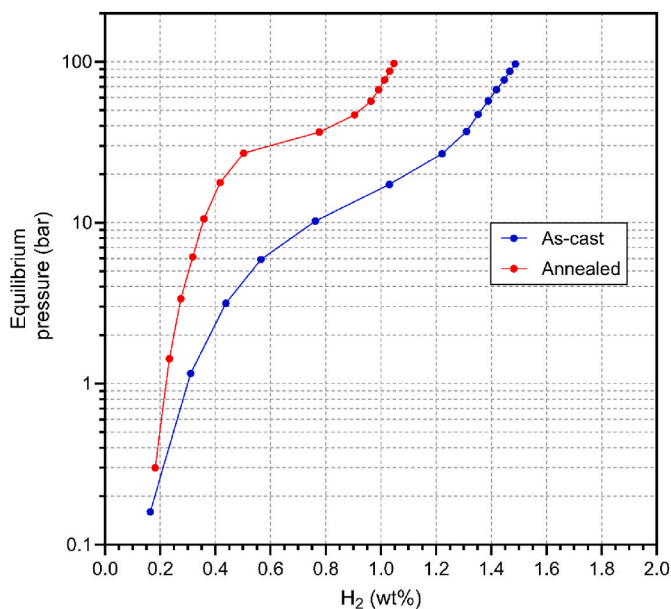


Fig. 12. Pressure-composition isotherms at 253 K of the as-cast and annealed samples of $\text{TiCr}_{1.64}$.

Levinger [34], and highlighted d spacing values for a binary Ti–Cr alloy (66 % Cr) annealed for 20 min at 1385 °C and water quenched. It is likely the produced C14 phase contained vacancies similar to those in this study, hence the reduction in unit cell volume compared to the COD. The COD reference for the C14 phase corresponds to a 1970 paper by Svechnikov et al. [35]. It is referenced and discussed in Murray’s paper [36], which details the Ti–Cr phase diagram and its construction, with a key comment being “because of difficulties in achieving equilibrium, the compound region of the phase diagram must still be regarded as speculative”. It is postulated that the COD reference, stemming from Svechnikov et al. [35], may have had limited vacancies, or was much closer the equilibrium than that of the ICDD reference, however, without the quantitative information, this is speculative. The same can be seen for the C15 Laves phase quantification. The COD C15 entry (1525361) exhibits a unit cell volume of 336.3 \AA^3 compared to the ICDD entry (03-065-4160) 334.7 \AA^3 . Again, the COD entry is referenced to the work of Svechnikov et al. [35], and hence the same reasoning above applies. Similarly, the ICDD entry, which referenced the work by Duwez and Taylor [37], was not accessible, however, it was cited in a larger report by Kessler et al. [38], and highlighted that “high temperature modification of TiCr_2 above 1300 °C, exhibited a hexagonal structure, whereas, the low temperature modification of TiCr_2 is cubic. The existence of allotropy in TiCr_2 , of course, means a more complicated set of phase relationships in this general region than if the phase were monomorphic”. Again, this leads to the assumption that variances seen between the COD and ICDD databases is likely due to vacancy variations, and hence the perceived differences in unit cell volume. A later Svechnikov paper in 1972 [39] highlighted the phase transformations in chromium-titanium compounds, referencing the Duwez and Taylor paper [37]. Despite a diffraction pattern being present, unfortunately the angle of reflection was not defined. This highlights the potential for discrepancies to arise in the generation of the database values and hence the larger disparity between the COD and ICDD files. This error is likely compounded when considering the other factors highlighted above such as the processing of the alloy, phase purity and whether annealing is employed.

The phase quantification from Rietveld refinement shows an increase in Ti phase percentage and a decrease in the C14 phase percentage as the Ti content in the alloy increases. This can be explained by examining into the Ti–Cr phase diagram. When looking above the $\gamma\text{-TiCr}_2/\beta\text{-TiCr}_2$ boundary at 1545 K on Fig. 8, the $\text{TiCr}_{1.78}$ and $\text{TiCr}_{1.85}$ alloys sit in the

$\gamma\text{-TiCr}_2$ region, whereas the $\text{TiCr}_{1.64}$ and $\text{TiCr}_{1.55}$ alloys sit in the $\beta\text{-Ti} + \gamma\text{-TiCr}_2$ region, explaining the presence of additional Ti in the $\text{TiCr}_{1.64}$ and $\text{TiCr}_{1.55}$ alloys. The greater C14 presence in the as-cast alloys richer in Cr interestingly then corresponds to a lesser C15 presence in the corresponding annealed alloys, according to the data presented in Table 5. It is notable that this is not the case for the alloys richer in Ti ($\text{TiCr}_{1.55}$ and $\text{TiCr}_{1.64}$), where the Laves phase percentages are similar. The alloy where C15 is most abundant, $\text{TiCr}_{1.64}$, sits very close to the $\alpha\text{-TiCr}_2/\beta\text{-Ti} + \alpha\text{-TiCr}_2$ boundary, as well as having less C14 phase to transform initially in comparison with the $\text{TiCr}_{1.78}$ and $\text{TiCr}_{1.85}$ alloys, which results in the best conversion to the C15 phase post-annealing.

The substitution of Ti for Cr into the C14 lattice can be linked to the observed hydrogen storage properties of the as-cast alloys. The alloys with a greater Ti content have a greater maximum storage capacity and lower plateau pressure. The difference in hydrogen storage capacity between the $\text{TiCr}_{1.55}$ and $\text{TiCr}_{1.64}$ as-cast alloys is 0.01 wt% at 253 K and so within error of measurement. This when coupled with the C14 lattice data from Rietveld refinement, suggests that there is a limit to how much Ti can improve the hydrogen storage properties of the C14 Laves phase. This is due to the Ti occupancy at the B sites in the C14 lattice does not continue to increase past the $\text{TiCr}_{1.64}$ alloy, as well as the overall cell volume increase between $\text{TiCr}_{1.64}$ and $\text{TiCr}_{1.55}$ being very small.

Annealing of the as-cast alloys has successfully reduced the quantities of minor phases for the case of the $\text{TiCr}_{1.64}$ alloy. In comparison with the first anneal at 1073 K with a duration of 2.5 days, there is a clear reduction in the constituent peaks of the Ti and Cr minor phases at $2\theta = 40^\circ$ and $2\theta = 44^\circ$ in the XRD pattern of the $\text{TiCr}_{1.64}$ alloy annealed at 1273 K for 14 days. The presence of the pure Cr is significantly reduced between the two annealed plots, however the small peak that is still present in the annealed alloys, as well as the calculated Cr weight percentage from Rietveld refinement, highlight that the rate of transition to the C15 is slow suggesting a longer period of annealing beyond 14 days is needed to maximise conversion to the C15 phase. The other benefit of annealing on the hydrogen storage properties of the alloy is the flattening of the plateau slope, which is more obvious at the beginning of the $\alpha + \beta$ phase as seen in Fig. 12. This is however counteracted by the observed loss in hydrogen storage capacity between the annealed and as-cast alloys.

Phase quantification from Rietveld refinement involving more than one Laves phase, and in this case with the Ti and Cr single phases, is challenging for both the as-cast and annealed alloys as several peak positions are shared between the observed phases in all the Ti–Cr alloys. This is especially true of the C14 and C15 Laves phases, where all the major peaks of the C15 phase (above relative intensity of 20 %) are overlapping or very close in position to major peaks of the C14 phase. The major Ti and Cr peaks also overlap with those of the C14 Laves phase. Whilst every effort has been made to carry out accurate Rietveld refinements with a well-considered methodology, the reasons stated above as well as the broader XRD peaks, particularly those in Fig. 3 of the as-cast alloys, means it is difficult to accurately quantify percentage changes of phases between the as-cast and annealed alloys. This is noted in other studies based on the Ti–Cr system [29].

There is a distinct decrease in the hydrogen storage capacity of the annealed $\text{TiCr}_{1.64}$ alloy in comparison to the as-cast. It is possible that during the annealing process, the excess Cr present in the as-cast alloys has diffused back into the C15 lattice during its formation from the C14 phase, perhaps into the Cr vacancies caused by off-stoichiometry. As a result, the C15 phase is more Cr-rich resulting in a negative effect on the hydrogen storage properties of the alloy. This is evidenced primarily from Rietveld refinement, where there is a substantial increase in Cr B-site occupancy between the C14 phase in the as-cast alloy (weighted average of 0.836) and the C15 phase in the annealed alloy (0.934). Phase quantification shows a reduction in residual Cr, as the Cr phase weight percentage also reduces from 10.4 % to 7.1 % between the as-cast and annealed $\text{TiCr}_{1.64}$ alloys. The increase in Cr in the C15 lattice leads to a reduced hydrogen storage capacity and an increased plateau

pressure, both of which can be seen in Fig. 12. At higher Ti substitution of Cr, there are more A2B2 tetrahedral sites, which are more favourable for H absorption. Through annealing, this allows diffusion of Cr from pure Cr into TiCr_{2-x} domains. This is further supported by EDX measurements, where the ratio of Cr to Ti in the Ti–Cr bulk areas increases from 1.774 to 1.816. It is also seen that the Ti-rich areas in the as-cast $\text{TiCr}_{1.64}$ alloy become even richer in Ti post-annealing, from a weight percentage of 58.9 % in the as-cast to 72.2 % in the annealed alloy.

The second cause of the observed reduction in hydrogen storage capacity between the as-cast and annealed $\text{TiCr}_{1.64}$ alloy is the increase of oxygen content in Ti-rich areas of the alloys. As seen in Table 6, the measured weight percentage of O increases from 16.6 % to 23.3 % in the Ti-rich areas. It is well known that O is a contaminant in hydrogen storage alloys, therefore this increase will have contributed towards the observed decrease in the storage capacity and potentially the initial activation of the annealed alloy.

5. Conclusions

Off-stoichiometric Ti–Cr AB_2 -based alloys have been synthesised and studied for their structural and hydrogen storage properties. The following main conclusions can be drawn from the results and analysis conducted from this study:

- Annealing is required to reduce the presence of minor phases (α -Ti, β -Cr) present from the initial arc melting, however, this process requires greater than two weeks in order to achieve maximum phase purity.
- The C14 cell size for the as-cast and C15 cell size for the annealed alloys both increase with Ti content, however no increase is observed past approximately Cr/Ti = 1.6.
- The increase in cell size indicates Ti substitution in the lattice, the observed trend indicates there is a limit to Ti B-site substitution.
- There is an initial drop-off in cell size between the stoichiometric TiCr_2 and $\text{TiCr}_{1.85}$ for both the C14 and C15 phases, suggesting that Cr vacancies are present in smaller deviations away from AB_2 stoichiometry, which may be because of thermal treatment.
- Alloys with a greater Ti content have a better maximum hydrogen storage capacity and lower plateau pressure.
- The reduction in hydrogen storage capacity of the annealed $\text{TiCr}_{1.64}$ alloy is owed to diffusion of residual Cr in the alloy into the C15 Laves phase during the annealing process (supported by the reducing Cr peak in XRD data) and increasing O content in Ti-rich areas.

Declaration of competing interest

The authors declare that they have no known competing financial interests or personal relationships that could have appeared to influence the work reported in this paper.

Acknowledgements

This work was graciously funded by the Engineering and Physical Sciences Research Council (EPSRC) through the EPSRC Centre for Doctoral Training in Sustainable Hydrogen (EP/S023909/1), and EPSRC Research Grants (EP/V042556/1 and EP/L022494/1). The authors would like to thank all technical help within the Wolfson building (XRD: Dr. Hannah Constantin) and the Nanoscale and Microscale Research Centre (nmRC) facilities (SEM/EDX) at the University of Nottingham. The authors would also like to thank LCM Ltd. for sponsoring this project.

References

- [1] Chen Z, Xiao X, Chen L, Fan X, Liu L, Li S, Ge H, Wang Q. Development of Ti–Cr–Mn–Fe based alloys with high hydrogen desorption pressures for hybrid hydrogen storage vessel application. *Int J Hydrogen Energy* 2013;12803–10.
- [2] Dehouche Z, Grimard N, Laurencelle F, Goyette J, Bose T. Hydride alloys properties investigations for hydrogen sorption compressor. *J Alloys Compd* 2005;399(1–2): 224–36.
- [3] Manickam K, Grant D, Walker G. Optimization of AB₂ type alloy composition with superior hydrogen storage properties for stationary applications. *Int J Hydrogen Energy* 2015;40(46):16288–96.
- [4] Pickering L, Lototskiy M, Davids M, Sita C, Linkov V. Induction melted AB₂-Type metal hydrides for hydrogen storage and compression applications. *Mater Today: Proc* 2018;5:10470–8.
- [5] Rusman N, Dahari M. A review on the current progress of metal hydrides material for solid-state hydrogen storage applications. *Int J Hydrogen Energy* 2016;41(28): 12108–26.
- [6] Sakintuna B, Lamari-Darkrim F, Hirscher M. Metal hydride materials for solid hydrogen storage: a review. *Int J Hydrogen Energy* 2007;32(9):1121–40.
- [7] Shibuya M, Nakamura J, Akiba E. Hydrogenation properties and microstructure of Ti–Mn-based alloys for hybrid hydrogen storage vessel. *J Alloys Compd* 2008;466 (1–2):558–62.
- [8] Tarasov B, Fursikov P, Volodin A, Bocharnikov M, Shimkus Y, Kashin A, et al. Metal hydride hydrogen storage and compression systems for energy storage technologies. *Int J Hydrogen Energy* 2021;46(25):13647–57.
- [9] Ulmer U, Dieterich M, Pohl A, Dittmeyer R, Linder M, Fichtner M. Study of the structural, thermodynamic and cyclic effects of vanadium and titanium substitution in laves-phase AB₂ hydrogen storage alloys. *Int J Hydrogen Energy* 2017;42(31):20103–10.
- [10] Yadav T, Shahi R, Srivastava O. Synthesis, characterization and hydrogen storage behaviour of AB₂ (ZrFe₂, Zr(Fe 0.75V 0.25)₂, Zr(Fe 0.5V 0.5)₂ type materials. *Int J Hydrogen Energy* 2012;37(4):3689–96.
- [11] Sandrock G, Sedriks J. State-of-the-Art review of hydrogen storage in reversible metal hydrides for military fuel cell applications. Ringwood, NJ: SunaTech Inc.; 1997.
- [12] Sandrock G. A panoramic overview of hydrogen storage alloys from a gas reaction point of view. *J Alloys Compd* 1999:877–88.
- [13] Machida Y, Yamada Y, Asanuma M. Hydride formation of C14-type Ti alloy. In: Hydrides for energy storage. Geilo; 1978.
- [14] Johnson J, Reilly J. Reaction of hydrogen with the low-temperature form (C15) of TiCr_2 . *Inorg Chem* 1978;17(11).
- [15] Johnson JR. Reaction of hydrogen with the high temperature (C14) form of TiCr_2 . *J Less Common Metal* 1980;73(2):345–54.
- [16] Johnson JR, Reilly JJ, Reidinger F, Corliss LM, Hastings JM. On the existence of F. C.C. $\text{TiCr}_1.8\text{H}_{5.3}$. *J Less Common Metal* 1982;88:107–14.
- [17] Loh S, Grant D, Walker G, Ling S. Substitutional effect of Ti-based AB₂ hydrogen storage alloys: a density functional theory study. *Int J Hydrogen Energy* 2023;48 (35):13227–35.
- [18] Li Q, Peng Z, Jiang W, Ouyang L, Wang H, Liu J, Zhu M. Optimization of Ti–Zr–Cr–Fe alloys for 45 MPa metal hydride hydrogen compressors using orthogonal analysis. *J Alloys Compd* 2021;889:161629.
- [19] Cao Z, Zhou P, Xiao X, Zhan L, Li Z, Wang S, Chen L. Investigation on Ti–Zr–Cr–Fe based alloys for metal hydride hydrogen compressor at moderate working temperatures. *Int J Hydrogen Energy* 2021;46(41):21580–9.
- [20] Wang X, Liu H, Li H. A 70 MPa hydrogen-compression system using metal hydrides. *Int J Hydrogen Energy* 2011;36(15):9079–85.
- [21] Zhang Q, Lei Y, Yang X, Ren K, Wang Q. Annealing treatment of AB₂-type hydrogen storage alloys: I. Crystal structures. *J Alloys Compd* 1999;292(1–2): 236–40.
- [22] Young K, Nei J, Wan C, Denys R, Yartys V. Comparison of C14- and C15-predominated AB₂ metal hydride alloys for electrochemical applications. *Batteries* 2017;3(3):22.
- [23] Shoemaker D, Shoemaker C. Concerning atomic sites and capacities for hydrogen absorption in the AB₂ Friauf-Laves phases. *J Less Common Metal* 1979;68(1): 43–58.
- [24] Young K, Nei J, Huang B, Fetcenko M. Studies of off-stoichiometric AB₂ metal hydride alloy: Part 2. Hydrogen storage and electrochemical properties. *Int J Hydrogen Energy* 2011;36(17):11146–54.
- [25] Chen Z, Xiao X, Chen L, Fan X, Liu L, Li S, Ge H, Wang Q. Influence of Ti superstoichiometry on the hydrogen storage properties of $\text{Ti}_{1+x}\text{Cr}_{1.2}\text{Mn}_0.2\text{Fe}_{0.6}$ (x = 0–0.1) alloys for hybrid hydrogen storage application. *J Alloys Compd* 2014;585: 307–11.
- [26] Ghosh G. Thermodynamic and kinetic modeling of the Cr–Ti–V system. *J Phase Equil* 2002;23(4):310–28.
- [27] Chen K, Allen S, Livingston J. Stoichiometry and alloying effects on the phase stability and mechanical properties of TiCr₂-base laves phase alloys. *Mater Res Soc Symp Proc* 1995;364(2):1401–6.
- [28] Baumann W, Leineweber A. Solid solubility by anti-site atoms in the C36-TiCr₂ Laves phase revealed by single-crystal X-ray diffractometry. *J Alloys Compd* 2010; 505(2):492–6.
- [29] Biffi C, Demir A, Coduri M, Previtali B, Tuissi A. Laves phases in selective laser melted TiCr_{1.78} alloys for hydrogen storage. *Mater Lett* 2018;226:71–4.
- [30] Murashkina T, Syrtanov M, Laptsev R, Lider A. Cyclic stability of the C36-type TiCr₂ Laves phase synthesized in the abnormal glow discharge plasma under hydrogenation. *Int J Hydrogen Energy* 2019;44(13):6709–19.

- [31] Carrillo-Bucio JL, Tena-García JR, Armenta-García EP, Hernández-Silva O, Cabañas-Moreno JG, Suárez-Alcántara K. Low-cost sieverts-type apparatus for the study of hydriding/dehydriding reactions. *HardwareX* 2018;4.
- [32] Coduri M, Mauri S, Biffi C. A new method for simple quantification of Laves phases and precipitates in TiCr₂ alloys. *Intermetallics* 2019;109:110–22.
- [33] Liu J, Sun L, Yang J, Guo D, Chen D, Yang L, Xiao P. Ti-Mn hydrogen storage alloys: from properties to applications. *RSC Adv* 2022;12(55):35744–55.
- [34] Levinger B. High temperature modification of TiCr₂. *J Met* 1953;5:196.
- [35] Svechnikov V, Teslyuk M, Kocherzhinskii Y, Pet'kov V, Dabizha E. Three modifications of TiCr₂. *Dopov Akad Nauk Ukr RSR* 1970;32(9):837–41.
- [36] Murray J. The Cr-Ti (Chromium-Titanium) system. *Bullet Alloy Phase Diagrams* 1981;2:174–81.
- [37] Duwez P, Taylor J. A partial titanium-chromium phase diagram and the crystal structure of TiCr₂. *Trans. ASM* 1952;44:495.
- [38] Kessler HD, Rostoker W, Van Thyne RJ. Titanium phase diagrams. Wright Air Development Centre; 1953. p. 52–335.
- [39] Svechnikov VN, Kocherzhinsky JA, Petkov VV, Polenur AV, Guzei LS. Phase transformations in chromium-titanium compounds. *J Less Common Metal* 1972;29(3):329–32.